ATLAS NOTE

ATLAS-CONF-2012-151

November 9, 2012

Search for supersymmetry using events with three leptons, multiple jets, and missing transverse momentum in 13.0 fb^{-1} of pp collisions with the ATLAS detector at $\sqrt{s}$=8 TeV

The ATLAS Collaboration

Abstract

This note reports on a search for supersymmetry using events with three leptons, four or more jets, and missing transverse momentum. The search utilizes 13.0 fb^{-1} of proton-proton collision data collected at $\sqrt{s}$ = 8 TeV with the ATLAS detector at the Large Hadron Collider. The data are found to be in agreement with the Standard Model expectation. The result is interpreted in terms of two simplified supersymmetry models. For pair-production of gluinos that decay into top quarks and neutralino via off-shell top squarks ($pp \rightarrow \tilde{g}\tilde{g}$, $\tilde{g} \rightarrow \tilde{t}_1^* \bar{t}$, and $\tilde{t}_1^* \rightarrow \tilde{\chi}_1^0 t$), gluinos with masses lower than 860 GeV are excluded at 95% CL for a light neutralino. For pair-production of bottom squarks each decaying via $\tilde{b} \rightarrow t + \tilde{\chi}_1^{\pm}$ (where $\tilde{\chi}_1^{\pm} \rightarrow W^{\pm}\tilde{\chi}_1^0$), bottom squarks masses up to 430 GeV are excluded, depending on the assumptions on neutralino and chargino masses.

ATLAS-CONF-2012-151
12 November 2012

1 Introduction

Supersymmetry [1–9] (SUSY) is considered to be a promising extension of the Standard Model (SM) at the electroweak scale. Naturalness suggests that the SUSY partners of the top quark (stops), gluon (gluinos), and possibly bottom quark (sbottoms) could have masses below 1 TeV [10, 11]. Consequently, they could be produced with large cross sections at the Large Hadron Collider (LHC).

This note reports on a search for pair-production of gluinos and of bottom squarks. Two different hypotheses regarding the mass hierarchy of SUSY particles are made. In the first one, gluinos and neutralinos are the lightest SUSY particles, and pair-produced gluinos decay to $t\bar{t}$+$\tilde{\chi}_1^0$ final states via off-shell stops (see Fig. 1). The second SUSY scenario assumes that only pair-production of bottom squarks is relevant, and a sbottom decays only via a top quark and a chargino ($\tilde{\chi}_1^\pm \rightarrow W^\pm$+$\tilde{\chi}_1^0$). Figure 1 illustrates these two processes of interest. These models feature the production of four $W^\pm$ bosons from either top quark decays (gluino pair-production) or from top quark and chargino decays (bottom squark pair-production). The SUSY models considered assume R-parity [12–16] conservation, so that neutralinos escape direct detection and lead to imbalance in the transverse momentum of observed particles.

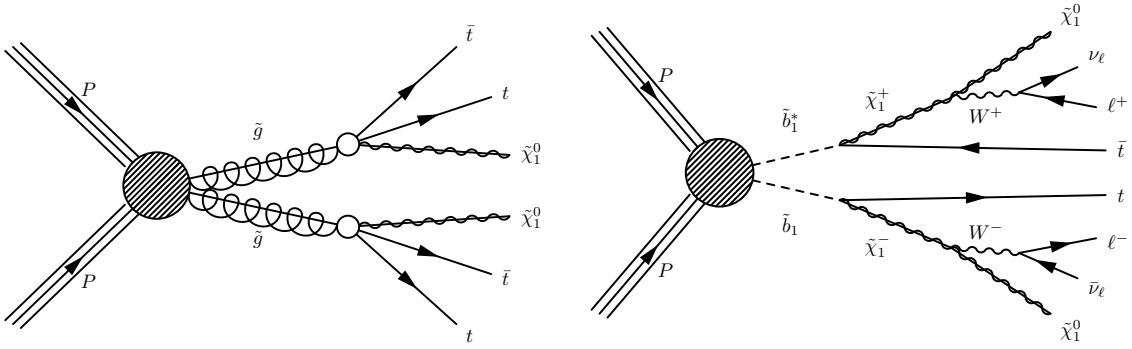

Figure 1: Diagrams for pair-production of gluinos (left) and bottom squarks (right).

The search is conducted as a counting experiment for events with three or more leptons, four or more hadronic jets, and missing transverse momentum. The leptons considered in this analysis are identified electrons and muons, including those from decays of tau leptons. The SM cross sections for production of background processes such as $t\bar{t}$+W, $t\bar{t}$+Z, $W^\pm Z$, ZZ, and three $W^\pm$ bosons are low, especially when additional jets are required. The selection of events with three or more leptons and multiple jets results in suppression of processes where hadronic jets are produced in association with $t\bar{t}$ or a Z boson. Therefore, final states with multiple W bosons decaying leptonically are a robust signature of new physics. The three-lepton events are separated into six categories depending on the charge-flavor combination of the three leptons[1] since the rates of the SM backgrounds and SUSY signal vary among the categories. The separation into these categories allows us to estimate contributions from processes where one lepton is non-prompt, from a hadron decay, or "fake", from mis-identification of a jet or a photon, and the other two leptons are prompt, from decays of on-shell W and Z bosons.

This note presents an update of the search carried out on the full 2011 dataset at $\sqrt{s}$=7 TeV proton-proton collisions [17] and is based on 13.0 fb^{-1} of data collected during the first part of 2012 by the ATLAS detector at $\sqrt{s}$=8 TeV. Results from other searches targeting the same SUSY scenarios have been made public by ATLAS [18–20] and CMS [21, 22].

[1]The first three leptons with the highest transverse momentum are considered. No requirement is imposed on additional leptons.

2 ATLAS detector

The ATLAS detector [23] consists of an inner tracking system (inner detector) surrounded by a thin superconducting solenoid providing a 2T magnetic field, electromagnetic (EM) and hadronic calorimeters, and a muon spectrometer. The inner detector consists of pixel and silicon microstrip detectors, surrounded by a straw tube transition radiation tracker. The electromagnetic calorimeter is a liquid argon and lead detector, split into barrel[2] ($|\eta| < 1.475$) and endcap ($1.375 < |\eta| < 3.2$) regions. Hadron calorimetry is based on two different detector technologies. The barrel ($|\eta| < 0.8$) and extended barrel ($0.8 < |\eta| < 1.7$) calorimeters are composed of scintillator and iron, while the hadronic endcap calorimeters ($1.5 < |\eta| < 3.2$) utilize liquid-argon and copper. The forward calorimeters ($3.1 < |\eta| < 4.9$) are instrumented with liquid-argon/copper and liquid-argon/tungsten, providing electromagnetic and hadronic energy measurements, respectively. The muon spectrometer is based on three large superconducting toroids arranged with an eight-fold azimuthal coil symmetry around the calorimeters, and a system of three stations of chambers for triggering and for precise track measurements.

3 Data sample

Candidate events were selected using triggers requiring at least two leptons (electrons and muons) with symmetric or asymmetric requirements on the lepton transverse energy or momentum. Tighter offline requirements on the lepton transverse energy and momentum ensure that the selected leptons are in the plateau region of high trigger efficiencies. All parts of the detector relevant to the measurement are required to be in good operating condition.

4 Monte Carlo simulation

Monte Carlo (MC) simulated event samples are used to develop and validate the analysis procedure and to evaluate the SM backgrounds in the signal region. The major SM contributions to events with three leptons, multiple jets, and missing transverse momentum are from $t\bar{t}$+jets (where additional isolated leptons are produced by b-quark decays or photon conversions), VZ+jets ($V = W$ or Z), and $t\bar{t}+V$+jets.

The modeling of multi-jet final states is of high importance for this analysis. The inclusive Z+jets, $Z+b\bar{b}$+jets, $Z+\gamma$+jets, $t\bar{t}$+jets, and VV+jets production is modeled using the Sherpa v1.4.1 [24] MC generator. As an alternative to Sherpa, the $t\bar{t}$+jets sample is simulated with PowHeg [25] plus Pythia [26]. The di-boson and $Z+\gamma$ samples from Sherpa contain matrix elements (MEs) for up to three final state partons. The $t\bar{t}$ and Z+jets samples instead contain ME calculations for up to four and five partons, respectively. The jet-parton matching is performed for 20 GeV jets using the CKKW [27, 28] procedure. The diboson samples, WZ, and ZZ, are generated with a $m(e^+e^-) > 0.1$ GeV cut-off. The inclusive Z+jets and $Z+\gamma$+jets samples have a cut-off of $m_Z > 40$ GeV. The overlap between the inclusive Sherpa Z+jets sample and the $Z+\gamma$+jets sample is removed manually using truth information on generated photons, while the overlap between the inclusive Sherpa Z+jets sample and the $Z+b\bar{b}$+jets sample is removed using truth b-jet multiplicity. A Z+light-flavor (LF) jets sample consists of events from the Z+jets sample that survived the overlap removal and from $Z+\gamma$+jets. The overlap removal procedure eliminated events with a b-quark jet with p_{T}>20 GeV or with a photon with p_{T}>10 GeV and minimum $\Delta R(\ell, \gamma) > 0.1$.

[2] ATLAS uses a right-handed coordinate system with its origin at the nominal pp interaction point (IP) in the center of the detector and the z-axis along the beam pipe. The x-axis points from the IP to the center of the LHC ring, and the y-axis points upward. Cylindrical coordinates (r, ϕ) are used in the transverse plane, ϕ being the azimuthal angle around the beam pipe. The pseudorapidity is defined in terms of the polar angle θ as $\eta = -\ln\tan(\theta/2)$ and the rapidity is defined as $y = \ln[(E + p_z)/(E - p_z)]/2$. The separation between final state particles is defined as $\Delta R = \sqrt{(\Delta y)^2 + (\Delta\phi)^2}$ and is Lorentz invariant under boosts along the z-axis. The transverse momentum is denoted as p_{T}.

By construction, the Z+LF jets sample includes c-quark jets. A Z+heavy-flavor (HF) jet sample consists of $Z+b\bar{b}$+jets events that have at least one truth b-jet with p_{T}>20 GeV. Single-top Wt production is simulated with MC@NLO [29]. MadGraph [30] is used to generate MEs for $t\bar{t}+V$+jets and VVV+jets, which are showered using Pythia.

The next-to-leading order (NLO) CT10 [31] parton density function (PDF) set is used for Sherpa, MC@NLO, and PowHeg. The CTEQ6L1 [32] set is used for MadGraph.

Theoretical cross section calculations at higher order are used to normalize the simulated processes. The next-to-next-to-leading order (NNLO) cross sections for inclusive production of Z bosons are taken from Ref. [33]. The corrections for the different thresholds of m_Z applied in the event generation are obtained with the MC simulations described earlier. The tree-level cross sections for Z+HF jets are scaled in proportion to the number of events that survived the removal of heavy flavor overlap. The corrected cross sections are multiplied by a K-factor of 1.23, using a conservative uncertainty of 55%. The $t\bar{t}$ cross section is calculated with Hathor at approximate NNLO accuracy [34] using the MSTW2008 NNLO PDF set [35] incorporating PDF+α_S uncertainties according to the MSTW prescription [36]. The diboson cross sections are documented in Ref. [37]. Again, the corrections for the different thresholds of m_Z in the ZZ and WZ MC simulations are obtained with the MC samples. The NNLO cross section calculation for Wt single-top production is described in Ref. [38]. The NLO cross sections for $t\bar{t}+W$ and $t\bar{t}+Z$ are taken from Refs. [39, 40] and the relative uncertainties on the cross-sections are 30% and 50% respectively. A K-factor of 1.5 is applied to cross sections for tri-boson production [41] and a conservative 100% uncertainty on the cross-section is used.

The SUSY signal samples are generated with HERWIG++ [42] using the PDF set CTEQ6L1. Signal cross sections are calculated to next-to-leading order in the strong coupling constant, adding the resummation of soft gluon emission at next-to-leading-logarithmic accuracy (NLO+NLL) [43–47]. The nominal cross section and the uncertainty are taken from an envelope of cross section predictions using different PDF sets and factorisation and renormalisation scales, as described in Ref. [48].

The MC samples are processed through a detector response simulation based on Geant4 [49] or a fast simulation based on the parameterisation of the performance of the ATLAS electromagnetic and hadronic calorimeters [50]. The simulated datasets are reweighted to match data using the average multiplicity of pp interactions that occurred in the bunch-crossings selected by the di-lepton triggers (in-time pileup).

5 Object definitions and event selection

5.1 Electron and Muon definitions

An electron candidate is reconstructed as a cluster of energy in the EM calorimeter, matched to a track in the inner detector. The track is fitted using a Gaussian-Sum Filter (GSF) [51] algorithm to account for bremsstrahlung energy losses. Electrons are required to have $p_{\mathrm{T}} > 15$ GeV and an absolute value of η of the electron calorimeter cluster to be less than 2.47. The p_{T} is calculated from the EM cluster energy and the pseudo-rapidity of the inner-detector track as $p_{\mathrm{T}} = E_{\mathrm{Cluster}} \cdot \sin(\theta_{\mathrm{track}})$. The electron cluster and track are required to satisfy requirements on the shape of the cluster, the quality of the track, angular matching between the track and the cluster, and the number of track hits in the innermost layer of the inner detector [52].

Muon candidates are required to have track segments in both the inner detector and the muon spectrometer. The two segments are combined using an algorithm which significantly reduces contamination from the decays-in-flight of light mesons [53,54]. A muon is required to have $p_{\mathrm{T}} > 15$ GeV and $|\eta| < 2.5$, with the momentum and pseudo-rapidity calculated using the combined track. The inner detector track must satisfy additional quality requirements.

To ensure that the leptons are promptly produced, the GSF-fitted track of an electron and the inner

detector segment of a muon track are required to originate from the primary vertex (see Section 5.4). The transverse impact parameter of the track d_0 and its significance $d_0/\sigma(d_0)$ are calculated with respect to the primary vertex. Similarly, the longitudinal impact parameter, z_0, is also calculated with respect to the primary vertex. For electrons, $|d_0/\sigma(d_0)| < 5$, and $|z_0| < 1$ mm are required. Similarly, for muons $|d_0| < 0.2$ mm, $|d_0/\sigma(d_0)| < 3$, and $|z_0| < 1$ mm are required.

In addition, electrons and muons must satisfy isolation requirements based on tracking and calorimeter information. The track-based isolation is achieved by requiring that the scalar sum of the transverse momenta of tracks, inside a cone of $\Delta R < 0.2$ around the lepton track, is less than 10% of the lepton p_{T}. The tracks considered in the sum must be compatible with the lepton vertex and have $p_{\mathrm{T}} > 0.4$ GeV (electrons) or $p_{\mathrm{T}} > 1$ GeV (muons). The calorimeter-based isolation requires that the transverse energy deposited in the calorimeter in a cone of radius $\Delta R < 0.2$ around the electron (muon), divided by the electron transverse energy (muon transverse momentum) is smaller than 0.2.

Corrections to the reconstruction efficiencies of leptons are applied to the simulated events. Corrections for trigger inefficiencies can be safely neglected given that the majority of selected events contain three leptons within the trigger acceptance.

5.2 Jet definition

For this analysis, jets are reconstructed using the FastJet implementation of the anti-k_t jet algorithm [55], with four-momentum recombination and a distance parameter $R = 0.4$. Jets are constructed from standard topological clusters [56], calibrated using the local cluster calibration (LC) [57] to account for various effects of non-compensation, dead material deposits and out-of-cluster deposits. Final jet energy scale corrections, and corrections for in-time and out-of-time pileup are also applied, as described in Ref. [58]. These corrections are derived using in situ techniques with data. Jets are required to have $p_{\mathrm{T}} > 30$ GeV and $|\eta| < 2.8$.

Jets entering the analysis are required to be separated by ΔR >0.2 from a selected lepton. A jet candidate is discarded if it lies within ΔR <0.2 of a lepton. This removes the effects of energy sharing or double-counting between the lepton and near-by jet. The effect is most pronounced in the electron channel.

To reject jets originating from pileup interactions, jets with $|\eta|$ <2.5 (fiducial to the tracking region) are required to have the ratio of the scalar sum of p_{T} of the associated tracks originating from the primary vertex to the scalar sum of p_{T} of all tracks associated to the jet, greater than 0.5.

5.3 Calculation of missing transverse momentum

The missing transverse momentum $E_{\mathrm{T}}^{\mathrm{miss}}$ is calculated as the magnitude of the vector sum of transverse momenta of the reconstructed jets, electrons, muons, and topological clusters that are not included in these objects. For this calculation, electrons are selected with $p_{\mathrm{T}} > 10$ GeV. Muons and electrons are required to satisfy all the baseline selection requirements except that of isolation. Jets are defined by the anti-k_t algorithm with $R = 0.4$ and are required to have $p_{\mathrm{T}} > 20$ GeV.

5.4 Event preselection

An initial sample of events containing three isolated leptons (electrons or muons) is selected as described below.

- **Data Quality** - All events are required to satisfy the data quality requirements described in Section 3. In addition, a set of cleaning requirements is applied to energy clusters in the calorimeter [59]. These reject events with a significant energy in the calorimeters from effects such as cosmic rays, beam-halo and beam-gas interactions, and instrumental noise.

- **Primary Vertex** - The primary vertex is required to have five or more associated tracks with $p_{\mathrm{T}} > 0.4$ GeV that are consistent with emerging from the beam spot. Interaction vertices are sorted in $\Sigma(p_{\mathrm{T}}^{\mathrm{track}})^2$, the sum of track ${p_{\mathrm{T}}}^2$, and the vertex with the maximum sum is selected as the primary vertex for this analysis.

- **Trigger** - Events are selected from the di-lepton trigger streams. In order to minimize uncertainties associated with the trigger efficiency each event is required to have at least one lepton in the plateau region of high efficiency. This corresponds to $p_{\mathrm{T}} > 20$ GeV for both electrons and muons.

- **Multi-lepton requirements** - Events are required to contain at least three isolated leptons that satisfy the requirements described in Section 5.1. Events with a pair of leptons having the same flavor, opposite charge, and $m(\ell^+\ell^-) < 12$ GeV are removed. The requirement removes events with pairs of energetic leptons from decays of heavy hadrons such as $J/\psi \to \ell^+\ell^-$. Its impact on the signal acceptance is negligible. Two leptons are considered to overlap if $\Delta R(\ell_1, \ell_2) < 0.1$. An overlapping electron and muon are both excluded, as is the softer of two overlapping electrons. No cases of two overlapping muons have been observed.

5.5 Final event selection and definition of the tri-lepton sample

The final tri-lepton sample is derived from the preselected sample with some additional requirements. After removing overlaps between reconstructed objects, the leptons are ordered in p_{T} to apply additional selection and classification requirements. The total charge of the first three leptons is required to be ± 1. This follows from the fact that the SUSY scenarios targeted in this analysis present a signature with four W bosons of net charge equal to zero, and hence the selection of any three should have a net charge of ± 1.

Additional requirements are imposed on an electron present among the three leptons. These requirements are only applied to the softest electron which has the same charge as the net charge of the three leptons. Constraints are imposed on the ratio between the energy of the electron cluster and the momentum of the track, E/p, and on the track-cluster match in ϕ. Criteria to suppress photon conversions are also applied.

To evaluate contributions from $t\bar{t}$+jets, Z+jets, WW+jets, and Wt+jets the events are classified into six categories depending on the number of observed electrons and the charge of the same-flavor pair when the third lepton is of a different flavor. Only the three leading leptons are used in the classification. Events with additional reconstructed leptons are kept. These charge/flavor categories are as follows:

- **3μ** - events with three muons and no electrons,

- **1e2OSμ** - events with an electron and two oppositely-charged muons,

- **1e2SSμ** - events with an electron and two same-charge muons,

- **2OSe1μ** - events with a muon and two oppositely-charged electrons,

- **2SSe1μ** - events with a muon and two same-charge electrons,

- **3e** - events with three electrons.

The SM backgrounds differ depending on the category, while the expected contributions from SUSY final states with four W bosons are similar for the six categories. Thus the population of these categories is an important indicator of the source of any signal. Typical values of the signal selection kinematic acceptance times detector efficiencies for the sum of the six categories are 0.9-1.8% for the pair-production of gluinos and 0.3-1.0% for sbottom pair-production. These values include the branching ratios for the leptonic decays of W bosons.

6 Signal and control regions

The tri-lepton events are divided into four non-overlapping kinematic regions, consisting of three control regions and a signal region. The control regions are used to estimate the SM backgrounds in the signal region. The regions are:

- **Z-boson control region** - Events have a pair of leptons with opposite charge, same flavor, and $81 < m(\ell^+\ell^-) < 101$ GeV.
- **Low-$E_{\mathrm{T}}^{\mathrm{miss}}$ control region** - Events have $E_{\mathrm{T}}^{\mathrm{miss}} < 50$ GeV and are not in the Z-boson control region.
- **$t\bar{t}$ control region** - Events have fewer than four jets, $E_{\mathrm{T}}^{\mathrm{miss}} > 50$ GeV, and are not in the Z-boson control region.
- **Signal region** - Events have four or more jets, $E_{\mathrm{T}}^{\mathrm{miss}} > 50$ GeV, and are not in the Z-boson control region.

Each region contains some or all of the six tri-lepton charge/flavor categories and the relative strength of the various background processes varies with category. The expected contamination of the control regions with the SUSY processes studied is low, with the $t\bar{t}$ control region being the most affected. The typical signal contamination is below 1%, the worst being about 7% for sbottom pair-production and $m(\tilde{b})$ ~400 GeV.

The dominant source of background is from processes with two real prompt leptons and a third misidentified lepton (referred to as "fake"). Processes likely to contribute to this background are $t\bar{t}$, WW, and Z final states accompanied by additional jets. A fake lepton can arise from the real, non-prompt decays of heavy hadrons, although these are suppressed by the lepton isolation requirement and the requirement on the transverse impact parameter of the track. Fake leptons can also arise from the misidentification of light hadrons as leptons and electrons can arise from misidentified conversions of photons. Again, these are suppressed by the lepton isolation and identification requirements. The probabilities of jets and photons faking a lepton are obtained from MC simulations and corrected with experimental data. The corrections are derived from data using the different charge-flavor populations in the control regions.

Another important source of tri-lepton events in the signal region is expected to be from SM processes leading to three prompt leptons. These are predominantly WZ, ZZ and $t\bar{t}$+V final states accompanied by additional jets. Their rates are calculated from MC simulation.

6.1 Estimation of fake lepton background

Sherpa samples are used to obtain predictions for events with a "fake" lepton in $t\bar{t}$, WW and Z final states accompanied by additional jets. Although the rates for fake leptons in the signal region are estimated by these calculations, the estimates are adjusted by introducing four scale factors which are determined from the data using various control regions.

The scale factors are different for electrons and muons, and depend on whether the fake originates from heavy-flavored or light-flavored hadrons. They are defined as follows:

- light-flavor jet faking an electron, $S(\mathrm{LF}\rightarrow e)$, (applied to Z+ LF jets and WW+jets),
- light-flavor jet faking a muon, $S(\mathrm{LF}\rightarrow \mu)$, (applied to Z+ LF jets and WW+jets),
- heavy-flavor jet faking an electron, $S(\mathrm{HF}\rightarrow e)$, (applied to Z + HF jets, Wt, and $t\bar{t}$),
- heavy-flavor jet faking a muon, $S(\mathrm{HF}\rightarrow \mu)$, (applied to Z+ HF jets, Wt, and $t\bar{t}$).

These corrections are applied to the normalization of the $t\bar{t}$, Z+ LF jets, Z+ HF jets, Wt, and WW+jets processes. Initially, the total yields of all background processes are normalized using the integrated luminosity and the predicted cross sections at the highest available accuracy. The expected rates for events with a "fake" lepton in a given tri-lepton category are multiplied by an appropriate linear combination of the electron and muon scale factors, $S(\text{process}\rightarrow \ell)$. The linear combinations are shown in Table 1.

Process	3μ	$1e2\text{OS}\mu$	$1e2\text{SS}\mu$	$2\text{OS}e1\mu$	$2\text{SS}e1\mu$	$3e$
Z+ LF jets, $Z\rightarrow ee$				$S(\text{LF}\rightarrow \mu)$	$S(\text{LF}\rightarrow \mu)$	$S(\text{LF}\rightarrow e)$
Z+ LF jets, $Z\rightarrow\mu\mu$	$S(\text{LF}\rightarrow \mu)$	$S(\text{LF}\rightarrow e)$	$S(\text{LF}\rightarrow e)$			
Z+ HF jets, $Z\rightarrow ee$				$S(\text{HF}\rightarrow \mu)$	$S(\text{HF}\rightarrow \mu)$	$S(\text{HF}\rightarrow e)$
Z+ HF jets, $Z\rightarrow\mu\mu$	$S(\text{HF}\rightarrow \mu)$	$S(\text{HF}\rightarrow e)$	$S(\text{HF}\rightarrow e)$			
$t\bar{t}$	$S(\text{HF}\rightarrow \mu)$	$S_c(\text{HF})$	$S(\text{HF}\rightarrow \mu)$	$S_c(\text{HF})$	$S(\text{HF}\rightarrow e)$	$S(\text{HF}\rightarrow e)$
Wt	$S(\text{HF}\rightarrow \mu)$	$S_c(\text{HF})$	$S(\text{HF}\rightarrow \mu)$	$S_c(\text{HF})$	$S(\text{HF}\rightarrow e)$	$S(\text{HF}\rightarrow e)$
WW+jets	$S(\text{LF}\rightarrow \mu)$	$S_c(\text{LF})$	$S(\text{LF}\rightarrow \mu)$	$S_c(\text{LF})$	$S(\text{LF}\rightarrow e)$	$S(\text{LF}\rightarrow e)$

Table 1: The multiplicative fake-rate scale factors are applied to the simulated processes depending on the flavors and charges of the final-state leptons. Since some processes contribute through both fake electrons and muons, the linear combinations $S_c(\text{HF}) = \{\epsilon_e \cdot S(\text{HF}\rightarrow\mu) + \epsilon_\mu \cdot S(\text{HF}\rightarrow e)\}/(\epsilon_e+\epsilon_\mu)$ and $S_c(\text{LF}) = \{\epsilon_e \cdot S(\text{LF}\rightarrow\mu) + \epsilon_\mu \cdot S(\text{LF}\rightarrow e)\}/(\epsilon_e+\epsilon_\mu)$ are defined, where ϵ_e and ϵ_μ are the reconstruction efficiencies for electrons and muons obtained from simulation of $t\bar{t}$ events. The scale factors are not applied to WZ, ZZ, $t\bar{t}$+W, and $t\bar{t}$+Z samples.

A likelihood function is defined in terms of the four fake-rate scale factors and the Poisson probabilities based on the observed and expected numbers of events in binned distributions. Sixteen distributions are selected from the possible flavor and charge categories in the three control regions:

- four distributions of $E_{\text{T}}^{\text{miss}}$ for the flavor and charge categories in the Z-boson control region[3],
- four distributions of $E_{\text{T}}^{\text{miss}}$ for the flavor and charge categories excluding those with leptons of the same charge and flavor in the low-$E_{\text{T}}^{\text{miss}}$ control region,
- two distributions of jet multiplicity for the low-$E_{\text{T}}^{\text{miss}}$ control region for charge-flavor final states with two leptons of the same charge and flavor,
- six distributions of jet multiplicity for the flavor and charge categories in the $t\bar{t}$ control region.

The distributions are chosen for variables that provide the best separation between processes with three prompt leptons, and with a "fake" lepton. Distributions other than these sixteen are used to validate accuracy of the background simulations.

The central values of the scale factors are obtained using fourteen of the above distributions, removing the $1\text{e}2\text{OS}\mu$ and 3e distributions from the Z-boson control region. The systematic uncertainties on the central value are calculated by using all the sixteen distributions and by removing $1\text{e}2\text{OS}\mu$ and 3e distributions from the low-$E_{\text{T}}^{\text{miss}}$ control region. Since photon conversions contribute significantly to the electron fake rate, this procedure assesses the impact of uncertainties in QED radiation, which affect these categories and these control regions specifically.

The minimization of the negative log likelihood leads to scale factors that range from 0.8 to 1.9, with statistical uncertainties between 10% and 37%. Systematic uncertainties obtained using the procedure described above are below 7% for $S(\text{LF/HF}\rightarrow\mu)$, and are as large as 45% (60%) for $S(\text{LF}\rightarrow e)$ ($S(\text{HF}\rightarrow e)$). The large systematic uncertainties to the electron-related corrections are due to the uncertainties on

[3]The $\mathbf{1}e\mathbf{2SS}\mu$ and $\mathbf{2SS}e\mathbf{1}\mu$ final states do not enter the control region.

QED radiation in events with a Z boson. The statistical and systematic uncertainties on the scale factors are included as an uncertainty on the expected number of background events. An additional uncertainty on the rate of $t\bar{t}$ events in the signal region is assigned by repeating the background evaluation procedure using the $t\bar{t}$ samples from PowHeg+Pythia instead of Sherpa. This procedure allows us to estimate uncertainties on the fake-rate scale factors associated with the choice of MC generator to simulate parton showering and b-quark fragmentation, as well as uncertainties on the transfer factor from the $t\bar{t}$ control region to the signal region.

Table 2 shows the number of events expected from the SM backgrounds in the three control regions, before and after applying the fake-rate scale factors. Figure 2(a) provides the comparison of data with MC for the $E_{\mathrm{T}}^{\mathrm{miss}}$ distribution in events contributing to the Z-boson control region, after applying the fake rate correction factors. Figure 2(b) shows the corresponding jet multiplicities. As shown in the plots, the Z+jets, the WZ and ZZ channels dominate these distributions. Corresponding plots for the low-$E_{\mathrm{T}}^{\mathrm{miss}}$ and $t\bar{t}$ control regions are shown in Figures 3 and 4. Data and SM predictions are found in agreement for the control regions.

	Z-boson CR	low-$E_{\mathrm{T}}^{\mathrm{miss}}$ CR	$t\bar{t}$ CR
Z+jets and $Z+b\bar{b}$+jets	$630\ ^{+200}_{-160}$ (520)	$460\ ^{+200}_{-60}$ (520)	$56\ ^{+26}_{-27}$ (54)
$t\bar{t}$	$28\ ^{+8}_{-7}$ (17)	$45\ ^{+16}_{-14}$ (28)	$103\ ^{+31}_{-24}$ (64)
Wt	1±1 (1)	$5\ ^{+3}_{-2}$ (3)	$8\ ^{+4}_{-3}$ (5)
WW, WZ, and ZZ	1500±120 (1500)	452±35 (452)	145±17 (145)
$t\bar{t}$+V, $t\bar{t}$+WW, and VVV	31±12 (31)	7±4 (7)	18±9 (18)
Total SM	$2190\ ^{+240}_{-200}$ (2070)	$970\ ^{+210}_{-80}$ (1010)	$330\ ^{+51}_{-57}$ (287)
Data	2358	959	310

Table 2: Expected number of events from SM backgrounds after (before) applying the fake-rate scale factors, and number of events observed in data in the three control regions. Numbers are shown for the sum of six categories. Uncertainties on the backgrounds include statistical and systematic effects.

7 Systematic uncertainties

The dominant detector-related uncertainties, affecting both background and signal predictions, arise from the jet energy scale (JES) and jet energy resolution (JER). These are determined from in-situ measurements and simulations [58]. The uncertainties on JES include those due to the close-by jets [60], unknown jet flavor composition [61], and pileup interactions [62]. The JES uncertainty varies as a function of jet p_{T} and η, and ranges from $\sim$ 2.5% at 60 GeV in the central region to $\sim$ 14% below 30 GeV in the forward regions. The uncertainty increases monotonically with the absolute value of jet pseudo-rapidity. The uncertainty on the correction of the JES for pileup pp interactions is less than 1.5% per additional interaction for jets with p_{T}>50 GeV. The uncertainty on the JER ranges from 2% to 5% depending on the η and p_{T} of the jet. The altered jet energies are also propagated into the calculation of $E_{\mathrm{T}}^{\mathrm{miss}}$. The JES and JER uncertainties both result in $\sim$ 20% uncertainty on the number of expected SM events in the signal region.

One of the dominant contribution to the uncertainties on the background estimations also arises from the scale factors for the fake rates (see Section 6.1), particularly from $S(\mathrm{HF}\rightarrow e)$ which result in a 15% uncertainty on the background predictions. The uncertainty on the rate of $t\bar{t}$ events in the signal region, evaluated using the PowHeg+Pythia instead of Sherpa MC generator (see Section 6.1), amounts to $\sim$ 10%.

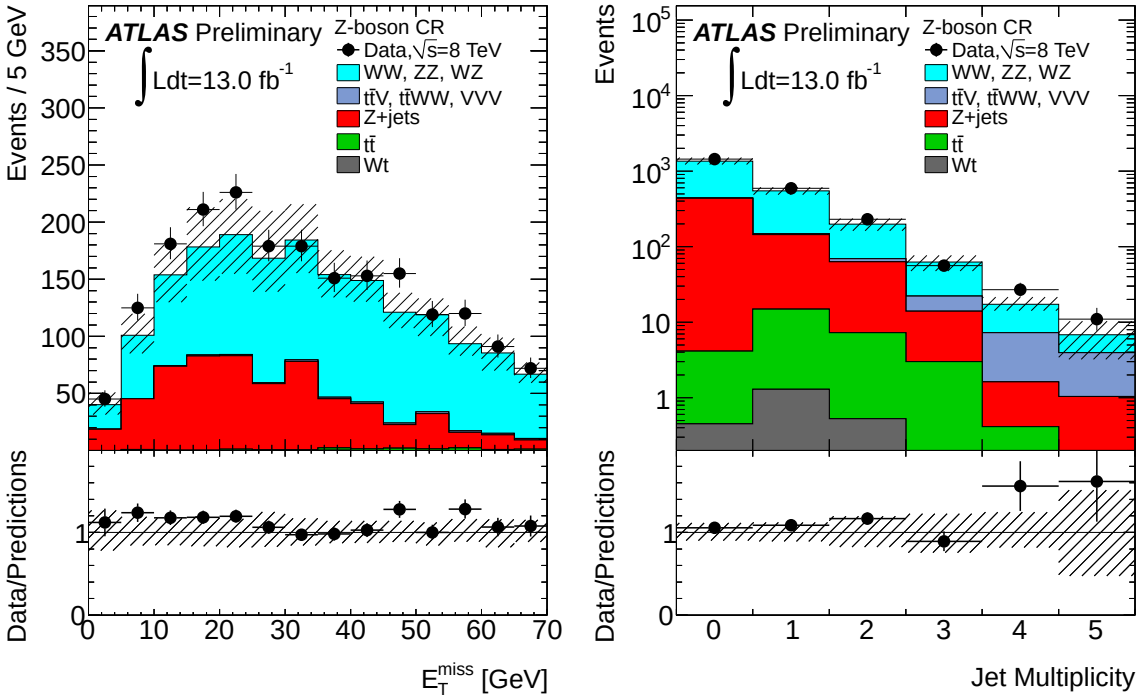

Figure 2: Distributions of $E_{\mathrm{T}}^{\mathrm{miss}}$ (left) and jet multiplicity (right) for events from the Z-boson control region. Fake-rate scale factors are applied to the $t\bar{t}$, Z+ jets, Wt, and WW+jets samples. The hashed band represents the sum of systematic uncertainties on the SM predictions.

Other important sources of uncertainties are due to the available statistics from MC simulations (12%), and theoretical uncertainties on cross sections of contributing processes (see Section 4). The latter results in $\sim$ 10% uncertainty on the background predictions.

The uncertainty on the integrated luminosity, measured using a technique similar to that of [63, 64]), is 3.6%. Uncertainties due to the lepton momentum/energy scale and resolution, and the data-driven scale factors for lepton efficiencies amount to $<$ 4% and $\sim$ 2% respectively. The uncertainty from pileup is estimated by varying rate of the pileup interactions in the simulated samples by 10% and results in 1% uncertainty on the background estimation. In addition, an uncertainty on the energy of clusters in the calorimeters not associated with a jet or electron, such as those from the underlying event and pileup interactions is also included. The effects are found to be negligible.

The detector-related uncertainties are also applied to the SUSY samples and amount to less than 5%. The dominant source is the uncertainty on luminosity followed by the uncertainties on the jet energy scale and efficiencies of lepton identification. These, however, are much smaller than the theoretical uncertainties on the signal cross section. In gluino-mediated stop models, theoretical uncertainties increase with the gluino mass, from 15% at $m_{\tilde{g}}$ = 400 GeV to over 30% for $m_{\tilde{g}}$ above 1000 GeV. They are dominated by uncertainties on the PDFs, which increase from about 10% to over 25% as the gluino mass increases. For the sbottom pair-production models, the uncertainties vary between 15% at $m_{\tilde{g}}$ = 300 GeV and 20% at $m_{\tilde{g}}$ = 800 GeV.

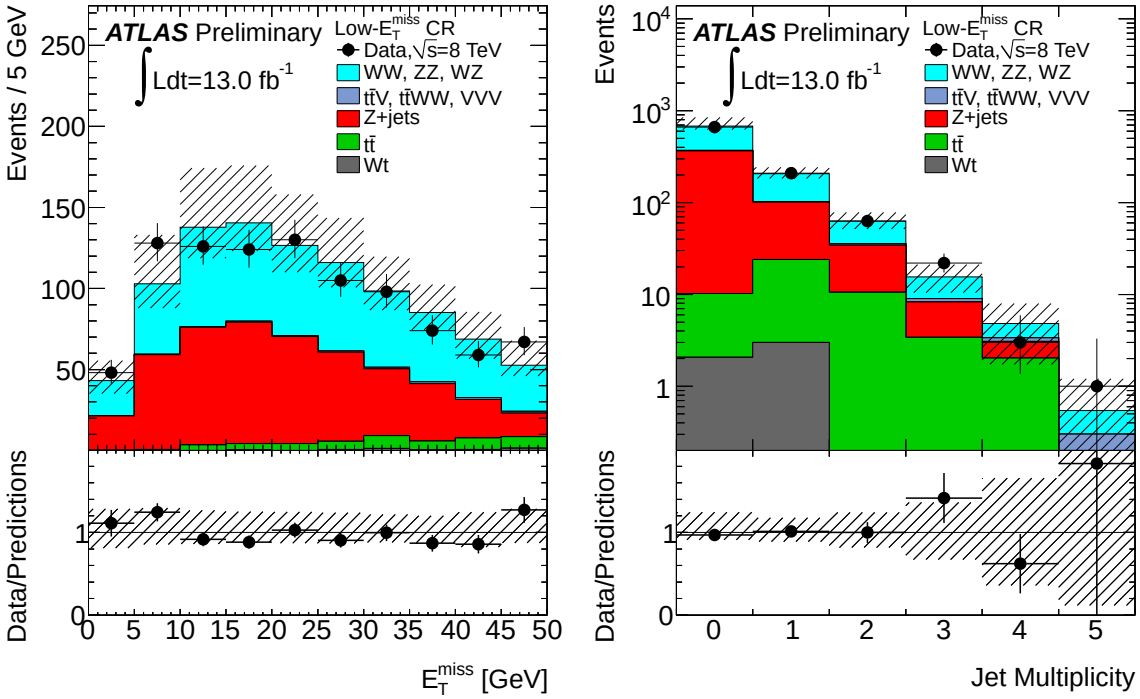

Figure 3: Distributions of $E_{\mathrm{T}}^{\mathrm{miss}}$ (left) and jet multiplicity (right) for events from the low-$E_{\mathrm{T}}^{\mathrm{miss}}$ control region. Fake-rate scale factors are applied to the $t\bar{t}$, Z+ jets, Wt, and WW+jets samples. The hashed band represents the sum of systematic uncertainties on the SM predictions.

8 Results and interpretation

The number of events observed in data and the number of expected events from SM backgrounds in the tri-lepton signal region and in each of the six categories are shown in Table 3. The $t\bar{t}$ production is the dominant background. Agreement between data and the expectation is observed in all individual categories and for their sum giving 14 events observed and $9.7\,^{+3.8}_{-3.4}$ (stat.⊕syst.) expected. Figure 5 shows distributions in jet multiplicity for data, SM predictions, and two representative SUSY models.

The CL_s prescription [65] is used to set a model independent upper exclusion limit at 95% confidence level (CL) on the number of signal events in the tri-lepton signal region, from the observed and expected numbers of events. Systematic uncertainties on the SM background predictions are included in the limit. An upper limit on the visible cross section (defined as cross section times kinematic acceptance times efficiency) of possible new physics processes is also derived. The observed (expected) upper limit on the number of signal events is 15.2 (11.5). The observed (expected) limit on the visible cross section is 1.2 (0.9) fb. The p-value for the background only hypothesis is 0.21.

The results are also interpreted in the context of the following SUSY simplified models:

- gluino-mediated stop production; $pp \to \tilde{g}\tilde{g}$, where gluinos always decay into two top quarks and a neutralino via a heavy off-shell stop: $\tilde{g} \to \tilde{t}\bar{t} \to t\bar{t}\,\tilde{\chi}_1^0$ and $m_{\tilde{t}}$=2.5 TeV. Exclusion limits are presented in the $m_{\tilde{g}} - m_{\tilde{\chi}_1^0}$ plane.

- direct sbottom production; $pp \to \tilde{b}\bar{\tilde{b}}$, where the sbottom always decays as $\tilde{b} \to t + \tilde{\chi}_1^{\pm}$ and the chargino subsequently decays as $\tilde{\chi}_1^{\pm} \to W^{\pm} + \tilde{\chi}_1^0$. Exclusion limits are presented in the $m_{\tilde{b}} - m_{\tilde{\chi}_1^0}$ plane, assuming $m_{\tilde{\chi}_1^{\pm}} = 2m_{\tilde{\chi}_1^0}$ and above the experimental LEP limit of about 104 GeV, and in the

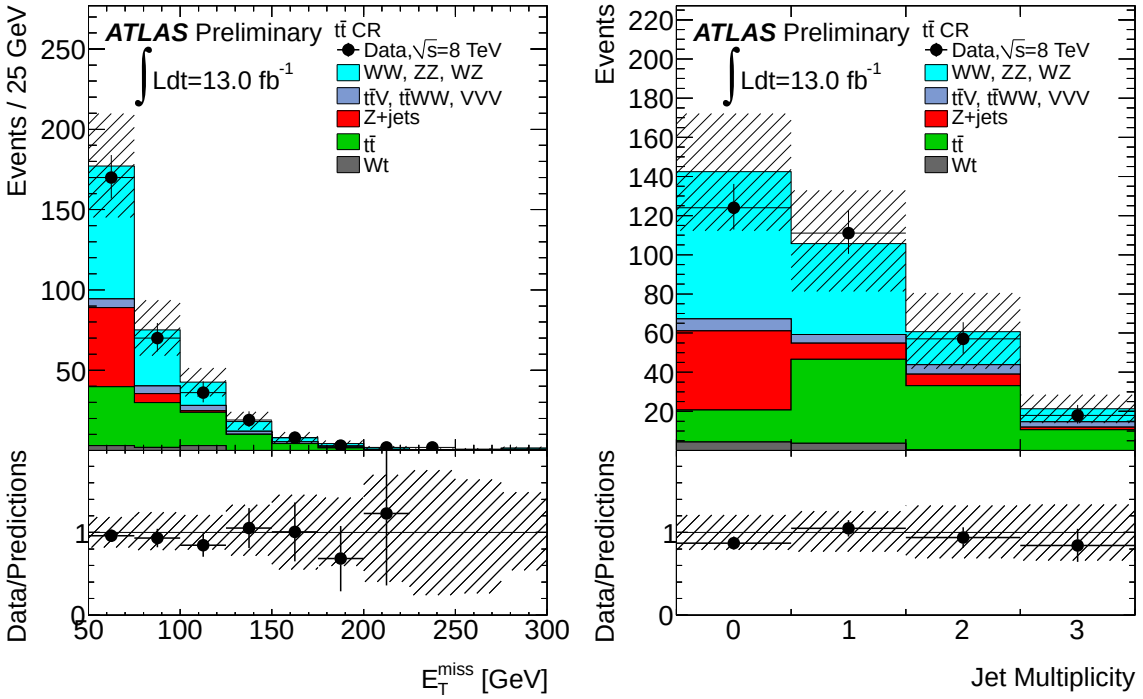

Figure 4: Distributions of $E_{\mathrm{T}}^{\mathrm{miss}}$ (left) and jet multiplicity (right) for events from the $t\bar{t}$ control region. Fake-rate scale factors are applied to the $t\bar{t}$, Z+ jets, Wt, and WW+jets samples. The right-most bin includes overflow. The hashed band represents the sum of systematic uncertainties on the SM predictions.

	3μ	$1e2\mathrm{SS}\mu$	$1e2\mathrm{OS}\mu$	$2\mathrm{SS}e1\mu$	$2\mathrm{OS}e1\mu$	$3e$	3ℓ
Z+jets and $Z+b\bar{b}$+jets	-	-	-	-	-	$0.4\,^{+0.4}_{-0.4}$	$0.4\,^{+0.4}_{-0.4}$
$t\bar{t}$ and Wt	0.7±0.8	0.5±0.5	$1.5\,^{+0.9}_{-0.8}$	$0.9\,^{+1.0}_{-0.9}$	$1.0\,^{+0.9}_{-0.8}$	$0.2\,^{+0.4}_{-0.2}$	$4.9\,^{+2.6}_{-2.0}$
WW, WZ, and ZZ	$0.7\,^{+0.4}_{-0.3}$	-	$0.8\,^{+0.3}_{-0.5}$	-	$0.3\,^{+0.3}_{-0.2}$	0.6±0.6	$2.4\,^{+1.3}_{-1.2}$
$t\bar{t}$+W and $t\bar{t}$+Z, and VVV	0.3±0.2	0.2 ±0.2	0.6±0.5	0.3±0.2	0.4±0.3	0.2±0.1	2.0±1.0
Total SM	1.8±1.0	0.8±0.5	2.9±1.2	$1.2\,^{+1.2}_{-1.0}$	$1.7\,^{+1.1}_{-1.0}$	$1.4\,^{+0.9}_{-0.8}$	$9.7\,^{+3.8}_{-3.4}$
Signal1	$1.3\,^{+0.4}_{-0.5}$	$1.2\,^{+0.3}_{-0.4}$	$2.2\,^{+0.6}_{-0.7}$	$1.2\,^{+0.3}_{-0.4}$	$2.2\,^{+0.6}_{-0.8}$	$0.7\,^{+0.2}_{-0.3}$	$8.9\,^{+2.2}_{-3.0}$
Signal2	0.9±0.3	$1.2\,^{+0.3}_{-0.4}$	$2.0\,^{+0.5}_{-0.6}$	$1.4\,^{+0.4}_{-0.5}$	2.0±0.6	$0.8\,^{+0.3}_{-0.3}$	$8.3\,^{+1.9}_{-2.3}$
Data	1	2	3	1	4	3	14

Table 3: Expected number of events from SM backgrounds and number of events observed in data in tri-lepton signal region. Expectations for two SUSY benchmark models for gluino mediated stop production with $m_{\tilde{g}}$=900 GeV and $m_{\tilde{\chi}_1^0}$=500 GeV (Signal1) and direct sbottom production with $m_{\tilde{b}}$=500 GeV, $m_{\tilde{\chi}_1^\pm}$=300 GeV and $m_{\tilde{\chi}_1^0}$=150 GeV (Signal2) are also shown. Numbers are shown for each of the six categories. Uncertainties on the backgrounds and SUSY signals include statistical and systematic uncertainties. Correlations between uncertainties are taken into account.

$m_{\tilde{b}} - m_{\tilde{\chi}_1^\pm}$ plane, assuming $m_{\tilde{\chi}_1^0}$=60 GeV.

Exclusion limits at 95% CL are calculated summing together the six categories in the tri-lepton signal region. Systematic uncertainties associated with jets, $E_{\mathrm{T}}^{\mathrm{miss}}$, pileup, leptons and luminosity are treated as fully correlated between signal and backgrounds. All other uncertainties are assumed to be uncorrelated.

The expected and observed exclusion limits at 95% CL are shown in Fig. 6. The yellow band around

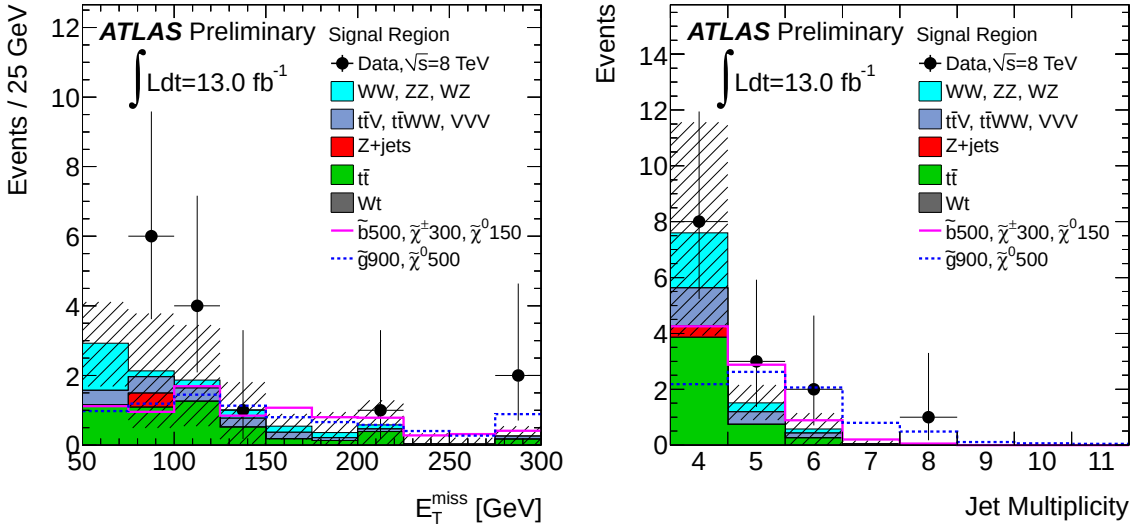

Figure 5: Distributions of $E_{\mathrm{T}}^{\mathrm{miss}}$ (left) and jet multiplicity (right) for events from the signal region. Fake-rate scale factors are applied to the $t\bar{t}$, Z+ jets, Wt, and WW+jets samples. The right-most bin includes overflow. The hashed band represents the sum of systematic uncertainties on the SM predictions. Expectations for two SUSY benchmark models for gluino mediated stop production with $m_{\tilde{g}}$=900 GeV and $m_{\tilde{\chi}_1^0}$=500 GeV and direct sbottom production with $m_{\tilde{b}}$=500 GeV, $m_{\tilde{\chi}_1^\pm}$=300 GeV and $m_{\tilde{\chi}_1^0}$=150 GeV are also shown.

the expected limit shows the $\pm 1\sigma$ results including all systematic uncertainties except the theoretical uncertainties on the SUSY cross section. The $\pm 1\sigma_{\mathrm{theory}}^{\mathrm{SUSY}}$ lines around the observed limit are obtained by changing the SUSY cross section by $\pm 1\sigma$ (where σ is defined as described in Section 4). All limits quoted later in this section are derived from the $-1\sigma_{\mathrm{theory}}^{\mathrm{SUSY}}$ line. Observed and expected limits obtained using 4.7 fb^{-1}of data collected in 2011 at $\sqrt{s}$=7 TeV [17] are shown by the blue lines.

Thanks to the low requirement on $E_{\mathrm{T}}^{\mathrm{miss}}$, the limit for gluino-mediated stop production only depends weakly on the neutralino mass. This search excludes models with gluino masses below 800 GeV and with neutralino masses $m_{\tilde{\chi}_1^0}$ <440 GeV on the line delimiting the area in which $\tilde{g} \to t\bar{t}\tilde{\chi}_1^0$ is kinematically not allowed. Gluino masses up to 860 GeV are excluded for low masses of neutralinos. Expected limits improve by about 100 GeV from the 7 TeV to the 8 TeVanalysis. Further improvements in the sensitivity are expected from a re-optimization of the signal region selection.

In direct sbottom production models, in the $m_{\tilde{b}} - m_{\tilde{\chi}_1^0}$ plane ($m_{\tilde{\chi}_1^\pm}$=2$m_{\tilde{\chi}_1^0}$), sbottom masses below 420 GeV are excluded for $m_{\tilde{\chi}_1^0}$=80 GeV. In the $m_{\tilde{b}} - m_{\tilde{\chi}_1^\pm}$ plane ($m_{\tilde{\chi}_1^0}$=60 GeV), sbottom masses of up to 430 GeV are excluded for chargino masses of 150 GeV to 210 GeV. The signal acceptance degrades when the mass separation between neutralino and chargino becomes low. It also decreases for low mass separation between sbottom squark and its decay products.

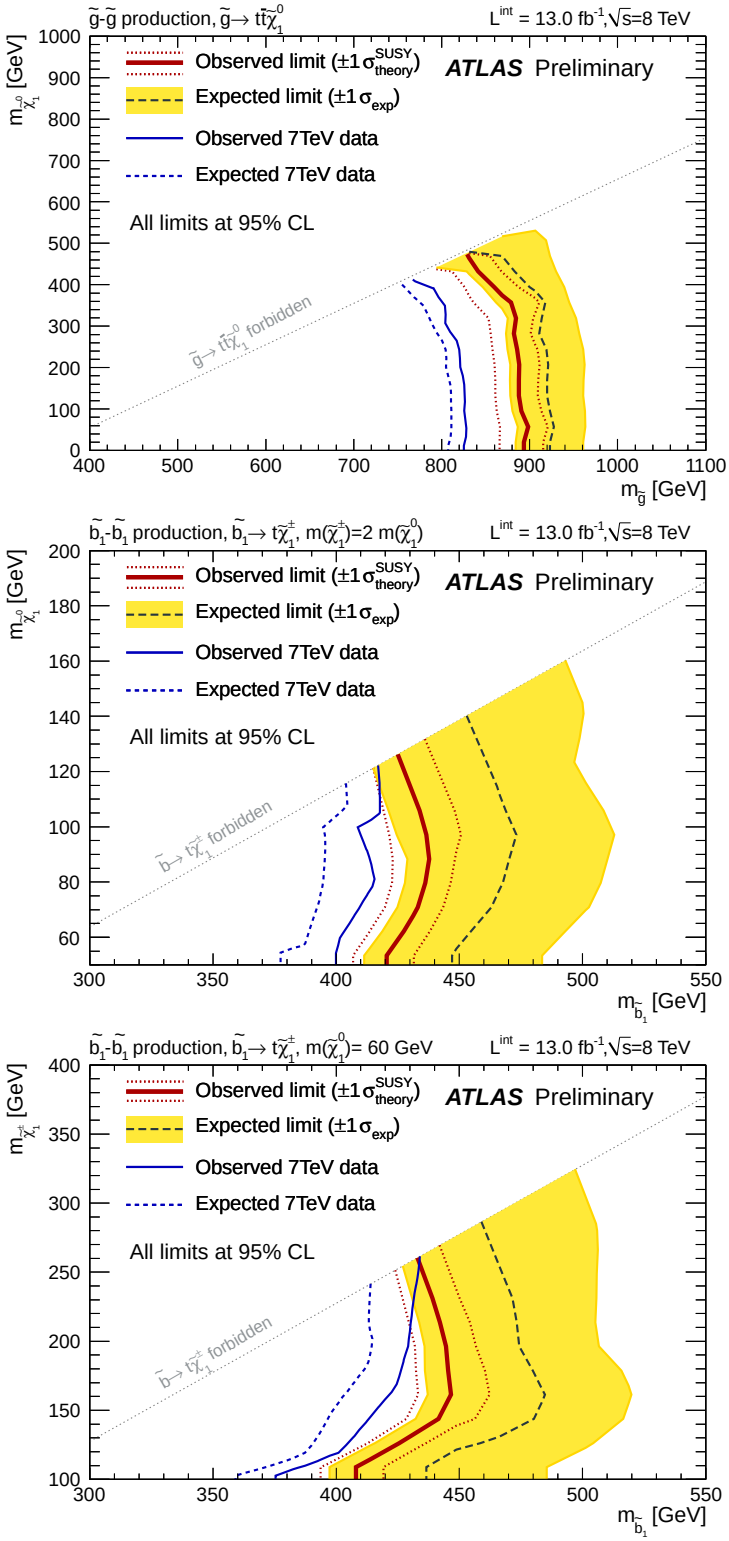

Figure 6: Expected and observed exclusion limit at 95% CL for gluino-mediated stop production in the $m_{\tilde{g}} - m_{\tilde{\chi}_1^0}$ plane (top) and direct sbottom production in the $m_{\tilde{b}} - m_{\tilde{\chi}_1^0}$ (middle) and $m_{\tilde{b}} - m_{\tilde{\chi}_1^\pm}$ (bottom) planes.

9 Conclusions

This note presents a search for supersymmetry in final states with three energetic leptons, multiple jets, and missing transverse momentum. The analysis is performed using 13.0 fb^{-1} of ATLAS data from proton–proton collisions at a center of mass energy of 8 TeV at the LHC collected in 2012.

The number of events observed in the signal region is found to be in agreement with the expectations from SM predictions. The results are interpreted in the context of simplified SUSY models. Exclusion limits at 95% CL are provided in the $m_{\tilde{g}} - m_{\tilde{\chi}_1^0}$ plane, for models where a gluino decays into two top quarks and a neutralino via an off-shell top squark. This analysis excludes neutralino masses below 440 GeV for gluino masses of 800 GeV.

Limits are also provided in the context of pair-production of bottom squarks where $\tilde{b} \rightarrow t + \tilde{\chi}_1^{\pm}$. Assuming a neutralino mass of 60 GeV, sbottom masses of up to 430 GeV are excluded for chargino masses of 150 GeV to 210 GeV.

References

[1] H. Miyazawa, *Baryon Number Changing Currents*, Prog. Theor. Phys. **36 (6)** (1966) 1266–1276.

[2] P. Ramond, *Dual Theory for Free Fermions*, Phys. Rev. D **3** (1971) 2415–2418.

[3] Y. A. Gol'fand and E. P. Likhtman, *Extension of the Algebra of Poincare Group Generators and Violation of p Invariance*, JETP Lett. **13** (1971) 323–326.

[4] A. Neveu and J. H. Schwarz, *Factorizable dual model of pions*, Nucl. Phys. B **31** (1971) 86–112.

[5] A. Neveu and J. H. Schwarz, *Quark Model of Dual Pions*, Phys. Rev. D **4** (1971) 1109–1111.

[6] J. Gervais and B. Sakita, *Field theory interpretation of supergauges in dual models*, Nucl. Phys. B **34** (1971) 632–639.

[7] D. V. Volkov and V. P. Akulov, *Is the Neutrino a Goldstone Particle?*, Phys. Lett. B **46** (1973) 109–110.

[8] J. Wess and B. Zumino, *A Lagrangian Model Invariant Under Supergauge Transformations*, Phys. Lett. B **49** (1974) 52.

[9] J. Wess and B. Zumino, *Supergauge Transformations in Four-Dimensions*, Nucl. Phys. B **70** (1974) 39–50.

[10] R. Barbieri and G. Giudice, *Upper Bounds on Supersymmetric Particle Masses*, Nucl. Phys. B **306** (1988) 63.

[11] B. de Carlos and J. Casas, *One loop analysis of the electroweak breaking in supersymmetric models and the fine tuning problem*, Phys. Lett. B **309** (1993) 320–328.

[12] P. Fayet, *Supersymmetry and Weak, Electromagnetic and Strong Interactions*, Phys. Lett. B **64** (1976) 159.

[13] P. Fayet, *Spontaneously Broken Supersymmetric Theories of Weak, Electromagnetic and Strong Interactions*, Phys. Lett. B **69** (1977) 489.

[14] G. R. Farrar and P. Fayet, *Phenomenology of the Production, Decay, and Detection of New Hadronic States Associated with Supersymmetry*, Phys. Lett. B **76** (1978) 575–579.

[15] P. Fayet, *Relations Between the Masses of the Superpartners of Leptons and Quarks, the Goldstino Couplings and the Neutral Currents*, Phys. Lett. B **84** (1979) 416.

[16] S. Dimopoulos and H. Georgi, *Softly Broken Supersymmetry and SU(5)*, Nucl. Phys. B **193** (1981) 150.

[17] ATLAS Collaboration, *Search for supersymmetry using events with three leptons, multiple jets, and missing transverse momentum with the ATLAS detector*, ATLAS-CONF-2012-108, CERN, Geneva, Aug, 2012.

[18] ATLAS Collaboration, *Search for new phenomena using large jet multiplicities and missing transverse momentum with ATLAS in 5.8 fb^{-1} of $\sqrt{s}$ = 8 TeV proton-proton collisions*, ATLAS-CONF-2012-103, CERN, Geneva, Aug, 2012.

[19] ATLAS Collaboration, *Search for Supersymmetry in final states with two same-sign leptons, jets and missing transverse momentum with the ATLAS detector in pp collisions at $\sqrt{s}$=8 TeV*, ATLAS-CONF-2012-105, CERN, Geneva, Aug, 2012.

[20] ATLAS Collaboration, *Search for top and bottom squarks from gluino pair production in final states with missing transverse energy and at least three b-jets with the ATLAS detector*, `arXiv:1207.4686 [hep-ph]`.

[21] CMS Collaboration, *Search for supersymmetery in final states with missing transverse momentum and 0, 1, 2, or ≥3 b jets in 8 TeV pp collisions*, CMS-PAS-SUS-12-016, 2012.

[22] CMS Collaboration, *Search for new physics in events with same-sign dileptons and b-tagged jets in pp collisions at $\sqrt{s}$=8 TeV*, CMS-PAS-SUS-12-017, CERN, Geneva, 2012.

[23] ATLAS Collaboration, *The ATLAS Experiment at the CERN Large Hadron Collider*, J. Instrum. **3** (2008) S08003.

[24] T. Gleisberg et al., *Event generation with SHERPA 1.1*, J. High Energy Phys. **02** (2009) 007.

[25] S. Frixion, P. Nason, and C. Oleari, *Matching NLO QCD computations with Parton Shower similations: the POWHEG method*, J. High Energy Phys. **11** (2007) 070.

[26] T. Sjöstrand, S. Mrenna, and P. Skands, *PYTHIA 6.4 physics and manual*, J. High Energy Phys. **05** (2006) 026.

[27] S. Catani and *et al.*, *QCD Matrix Elements + Parton Showers*, J. High Energy Phys. **11** (2001) 063, `arXiv:hep-ph/0109231`.

[28] S. Hoeche and *et al.*, *QCD matrix elements and truncated showers*, J. High Energy Phys. **05** (2009) 053, `arXiv:hep-ph/0903.1219`.

[29] S. Frixione and B. R. Webber, *Matching NLO QCD computations and parton shower simulations*, J. High Energy Phys. **06** (2002) 029.

[30] J. Alwall et al., *MadGraph/MadEvent v4: The New Web Generation*, J. High Energy Phys. **09** (2007) 028.

[31] H.-L. Lai et al., *New parton distributions for collider physics*, Phys. Rev. D **82** (2010) 074024.

[32] J. Pumplin et al., *New generation of parton distributions with uncertainties from global QCD analysis*, J. High Energy Phys. **07** (2002) 012.

[33] R. Gavin, Y. Li, F. Petriello, and S. Quackenbush, *FEWZ 2.0: A code for hadronic Z production at next-to-next-to-leading order*, Comput. Phys. Commun. **182** (2011) 2388–2403.

[34] M. Aliev et al., *HATHOR: HAdronic Top and Heavy quarks crOss section calculatoR*, Comput. Phys. Commun. **182** (2011) 1034–1046.

[35] A. D. Martin, W. J. Stirling, R. S. Thorne, and G. Watt, *Parton distributions for the LHC*, Eur. Phys. J. C **63** (2009) 189–285.

[36] A. D. Martin, W. J. Stirling, R. S. Thorne, and G. Watt, *Uncertainties on alpha(S) in global PDF analyses and implications for predicted hadronic cross sections*, Eur. Phys. J. C **64** (2009) 653–680.

[37] J. M. Campbell, R. K. Ellis, and C. Williams, *Vector boson pair production at the LHC*, J. High Energy Phys. **2011** (2011) 1–36.

[38] N. Kidonakis, *Two-loop soft anomalous dimensions for single top quark associated production with a W- or H-*, Phys. Rev. D **82** (2010) 054018.

[39] M. V. Garzelli et al., *$t\bar{t}W$ and $t\bar{t}Z$ Hadroproduction at NLO accuracy in QCD with Parton Shower and Hadronization effects*, arXiv:1208.2665 [hep-ph].

[40] J. M. Campbell and R. K. Ellis, *$t\bar{t}W$ production and decay at NLO*, arXiv:1204.5678 [hep-ph].

[41] F. Campanario, V. Hankele, C. Oleari, S. Prestel, and D. Zeppenfeld, *QCD corrections to charged triple vector boson production with leptonic decay*, Phys.Rev. **D78** (2008) 094012, arXiv:0809.0790 [hep-ph].

[42] M. Bahr et al., *Herwig++ Physics and Manual*, Eur. Phys. J. C **58** (2008) 639–707.

[43] W. Beenakker, R. Hopker, M. Spira, and P. Zerwas, *Squark and gluino production at hadron colliders*, Nucl. Phys. B **492** (1997) 51–103.

[44] A. Kulesza and L. Motyka, *Threshold resummation for squark-antisquark and gluino-pair production at the LHC*, Phys. Rev. Lett. **102** (2009) 111802.

[45] A. Kulesza and L. Motyka, *Soft gluon resummation for the production of gluino-gluino and squark-antisquark pairs at the LHC*, Phys. Rev. D **80** (2009) 095004.

[46] W. Beenakker, S. Brensing, M. Kramer, A. Kulesza, E. Laenen, et al., *Soft-gluon resummation for squark and gluino hadroproduction*, J. High Energy Phys. **12** (2009) 041.

[47] W. Beenakker, S. Brensing, M. Kramer, A. Kulesza, E. Laenen, et al., *Squark and gluino hadroproduction*, Int. J. Mod. Phys. A **26** (2011) 2637–2664.

[48] M. Krämer et al., *Supersymmetry production cross sections in pp collisions at $\sqrt{s}$=7 TeV*, arXiv:1206.2892 [hep-ph].

[49] GEANT4 Collaboration, S. Agostinelli et al., *GEANT4: A simulation toolkit*, Nucl. Instrum. Meth. Phys. Res., Sect. A **506** (2003) 250–303.

[50] ATLAS Collaboration, *The ATLAS Simulation Infrastructure*, Eur. Phys. J. C **70** (2010) 823–874.

[51] ATLAS Collaboration, *Improved electron reconstruction in ATLAS using the Gaussian Sum Filter-based model for bremsstrahlung*, ATLAS-CONF-2012-047, CERN, Geneva, May, 2012.

[52] ATLAS Collaboration, *Electron performance measurements with the ATLAS detector using the 2010 LHC proton-proton collision data*, Eur. Phys. J. C **72** (2012) 1909.

[53] ATLAS Collaboration, *Determination of the muon reconstruction efficiency in ATLAS at the Z resonance in proton-proton collisons at* $\sqrt{s}$*=7 TeV*, ATLAS-CONF-2011-008, CERN, Geneva, Feb, 2011.

[54] ATLAS Collaboration, *A measurement of the ATLAS muon reconstruction and trigger efficiency using* J/ψ *decays*, ATLAS-CONF-2011-021, CERN, Geneva, Mar, 2011.

[55] M. Cacciari, G. Salam, and G. Soyez, *The anti-*k_t *jet clustering algorithm*, J. High Energy Phys. **04** (2008) 063.

[56] W. Lampl et al., *Calorimeter Clustering Algorithms: Description and Performance*, ATL-LARG-PUB-2008-002, 2008.

[57] T. Barillari et al., *Local Hadron Calibration*, ATL-LARG-PUB-2009-001, 2009.

[58] ATLAS Collaboration, *Jet energy measurement with the ATLAS detector in proton-proton collisions at* $\sqrt{s}$*=7 TeV*, `arXiv:1112.6426 [hep-ex]`. submitted to Eur. Phys. J. C.

[59] ATLAS Collaboration, *Selection of jets produced in proton-proton collisions with the ATLAS detector using 2011 data*, ATLAS-CONF-2012-020, CERN, Geneva, Mar, 2012.

[60] ATLAS Collaboration, *Close-by Jet Effects on Jet Energy Scale Calibration in pp Collisions at* $\sqrt{s}$ *= 7 TeV with the ATLAS Detector*, ATLAS-CONF-2011-062, CERN, Geneva, Apr, 2011.

[61] ATLAS Collaboration, *Light-quark and Gluon Jets in ATLAS*, ATLAS-CONF-2011-053, CERN, Geneva, Apr, 2011.

[62] ATLAS Collaboration, *In-situ jet energy scale and jet shape corrections for multiple interactions in the first ATLAS data at the LHC*, ATLAS-CONF-2011-030, CERN, Geneva, Mar, 2011.

[63] ATLAS Collaboration, *Luminosity Determination in pp Collisions at* $\sqrt{s}$ *= 7 TeV using the ATLAS Detector in 2011*, ATLAS-CONF-2011-116, CERN, Geneva, Aug, 2011.

[64] ATLAS Collaboration, *Luminosity Determination in pp Collisions at* $\sqrt{s}$ *= 7 TeV using the ATLAS Detector at the LHC*, Eur. Phys. J. C **71** (2011) 1630.

[65] A. Read, *Presentation of search results: the CLs technique*, J. Phys. G: Nucl. Part. Phys. **28** (2002) 2693–2704.